

Analyses of steady and unsteady flows in a turbocharger's radial turbine

Mahfoudh Cerdoun¹ and Adel Ghenaïet²

Proc IMechE Part E:
J Process Mechanical Engineering
0(0) 1–16
© IMechE 2015
Reprints and permissions:
sagepub.co.uk/journalsPermissions.nav
DOI: 10.1177/0954408914566896
uk.sagepub.com/jpme



Abstract

This study presents the aerodynamic behaviours of a twin-entry radial inflow turbine under steady and transient conditions. The influence of the volute tongue is depicted by a low momentum wake propagating toward the rotor entry, but its effect does not extend beyond a circumferential position of 60°, and more total pressure loss is revealed with respect to the hub side. The transient simulations carried out at different operating conditions and Fast Fourier Transform analysis of static pressure fluctuations induced by the components' interactions have revealed a space-time periodic behaviour which has been described by a double Fourier decomposition. The flow simulations considering the two sides subject to both non-pulsatile and pulsatile flows conditions have revealed the existing rotor and tongue potential effects and interaction effects the rotor and volute, in addition to the circumferential and spanwise flow non-uniformities at the volute exit, which are more accentuated with a pulsatile flow at inlet. The results of Fast Fourier Transform analysis of temporal pressure fluctuations at the inter-space depict an unsteady behaviour related to the pulsatile frequencies which are characterised by high amplitudes. On the other hand, the spatial pressure fluctuations for the non-pulsatile and pulsatile flows conditions seem to have the same dominant modes since Fast Fourier Transform analysis was carried out at a fixed instant.

Keywords

Twin-entry radial turbine, aerodynamic performance, pressure fluctuations, pulsatile flows, Fast Fourier Transform analysis, volute/rotor interactions, potential effect

Date received: 18 March 2014; accepted: 27 November 2014

Introduction

Radial inflow turbines are widely used in the turbocharging of diesel engines owing to their capacity to absorb the residual energy from exhaust gases. For a single-entry volute, the flow rate of exhaust gas is low at lower engine speeds, and therefore the exhaust pressure at the gathering point of an exhaust manifold is low, resulting in a low boost pressure. By using a twin-entry radial inflow turbines there is a better recovery of energy from the pulsating exhaust gases. Despite they become extensively used in turbocharging, they only benefited from few studies as compared to single-entry radial turbines. Pischiger and Wunsche¹ studied twin-entry turbines under steady conditions and showed that unequal inlet conditions have a significant effect on the turbine performance. Also, Dale and Watson² indicated significant effects of partial and unequal admissions on both the swallowing capacity and efficiency of a twin-entry turbine, and showed that the maximum efficiency does not necessarily occur under equal admission, and these conclusions were also supported by the experiments of Capobianco and Gambarotta.³ Yeo and Baines^{4,5} extended the study of Dale and Watson using laser two-focus velocimetry techniques to examine the flow

inside a turbine, and showed that for different operating points and equal admission the flow incidence is close to -30° . Doppler velocimetry measurements by Karamanis et al.⁶ under steady and pulsating conditions revealed complex flow patterns at both inlet and exit and the unsteady performance have a substantial deviation from the performance and flow characteristics of steady state. Experimental results of two versions of a mixed-flow turbine were obtained by Hakeem et al.,⁷ which revealed that in the steady case, the use of a volute with a larger swallowing capacity may result in a higher isentropic efficiency at lower speeds and higher velocity ratios, whereas the unsteady case indicated that the instantaneous

¹Laboratory of Thermal Power Systems, Applied Mechanics, Ecole militaire polytechnique, BP17 Bordj-el-Bahri, 16046, Algiers, Algeria.

²Faculty of Mechanical and Process Engineering, University of Sciences and Technology, USTHB, BP32 El-Alia, Bab-ezzouar, 16111, Algiers, Algeria.

Corresponding author:

Adel Ghenaïet, Faculty of Mechanical and Process Engineering, University of Sciences and Technology, USTHB, BP32 El-Alia, Bab-ezzouar, 16111, Algiers, Algeria.
Email: ag1964@yahoo.com

performance and flow characteristics deviate substantially from their steady-state values. In the last two decades, the flow simulations in the support of turbomachinery design and development have grown to a considerable extent, as a consequence of the rapid evolution of computing power. By using CFX code, Simpson et al.^{8,9} showed that the vaned stators present a higher total pressure losses compared to equivalent vaneless volutes which exhibit higher levels of flow uniformity at rotor entry, yielding an improved turbine efficiency, which was also confirmed by the experimental investigations due Spence et al.¹⁰ The performance of a turbocharger's twin-entry radial turbine was investigated analytically and experimentally by Aghaali and Hajilouy-Benisi¹¹ and Hajilouy-Benisi et al.¹² under steady state, considering the full and partial admission. The results revealed that when the ratio of the shroud and hub side mass flows is very high, the efficiency is lower than that of the full admission. Hellström and Fuchs,¹³ in their first report presented numerical analyses for a vaneless turbine coupled to an IC engine operating at 1500 r/min and 3000 r/min, concluded that for the second speed, the inlet flow angle varies from approximately from -67° to -25° which is more favourable than for the first speed where this angle was from -85° to 60° accompanied with a drop in the peak shaft power about 4%. In their two other reports,^{14,15} a variety of non-pulsatile inlet boundary conditions including uniform flow and several combinations of turbulence with swirl and streamwise vortices were tested. As results, the undisturbed inlet profile gave the highest time-averaged power output while the performance of pulsating flow deviates subsequently from the steady one, as also confirmed later by Costall et al.,¹⁶ Copeland et al.¹⁷ Romagnoli et al.¹⁸ compared between the steady performance of double-entry and twin-entry turbocharger turbines, and showed that in the case of a twin radial turbine, the interaction between entries is significant and causes the flow capacity to be larger than that would be obtained by halving the mass flow in a full admission in contrary to the double-entry turbine.

The interaction phenomena between the rotor and the stationary components is considered to have a strong influence on the flow of a radial turbine and a better understanding is required in order to improve its

design. However, the knowledge about this influence is still not satisfactory when considering pulsatile flows. The present paper is concerned with the simulations of steady and unsteady flows through a twin-entry radial inflow turbine and the analyses of volute/rotor flow interactions. The aeroacoustic theory commonly used to identify the rotor/stator interactions in axial turbomachines^{19,20} is extended to the present study for analyzing such unsteadiness in the case of a twin-entry vaneless radial turbine. The attention is particularly directed to the inter-space local mixing flow between the two sides of volute entries, as it determines the intensity of interactions between the rotor and this twin-entry volute. The spectral analyses by the Fast Fourier Transform (FFT) for the different recorded static pressure signals revealed a space-time periodic behaviour that was described by the double Fourier decomposition and permitted to determine the different frequencies and prevailing modes, which allowed assessing the complex flows and the interactions phenomena through this type of a radial turbine.

CFD modelling

The studied twin-entry radial turbine (Figure 1) has 12 rotor blades with an inlet diameter of 96 mm and an external outlet diameter of 86.3 mm. The intake area of each entry is $2.263 \times 10^{-3} \text{ m}^2$. To take the three-dimensional (3D) measurements an optical measurement technique was used, which is equipped by an optical feeler and a three translation displacements in addition to a rotational chuck give for sweeping the totality of the surfaces. To reproduce the complex geometry of the rotor, a number of points located on the blade profiles were selected to get the correct shape. The volute was split into several parts to make an easy accessibility of the spot of light.

The grid of the volute has an hexahedral meshing refined in areas of high curvatures and gradients, particularly around the tongue and the rotor interfaces (Figure 2(a)). For the rotor domain, an H-grid topology is adopted with an O-grid wrapped around the blade to minimize skew angles and ensure a good boundary layer resolution. In the rotor tip clearance of 0.205 mm, 12 uniform cells are used to capture the

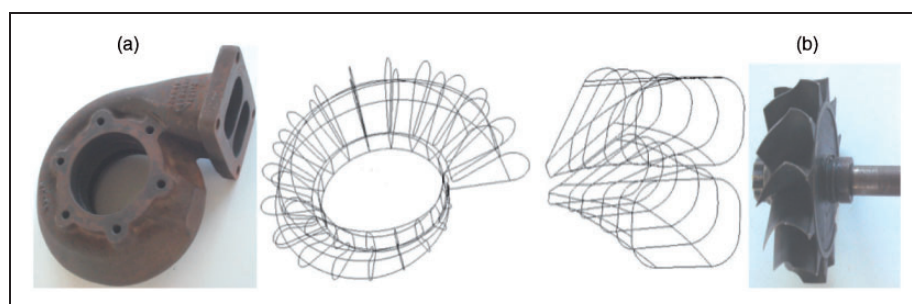


Figure 1. Geometry reproduction. (a) Splits of volute and two entries. (b) Rotor.

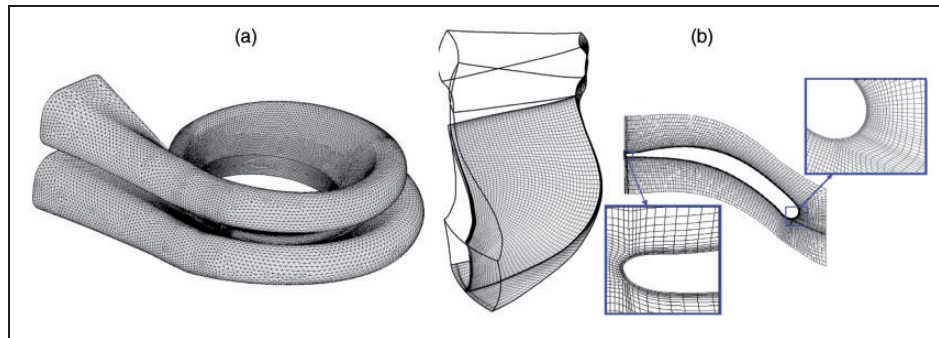


Figure 2. Turbine grid. (a) Volute grid. (b) Rotor, hub and mid-span meshes.

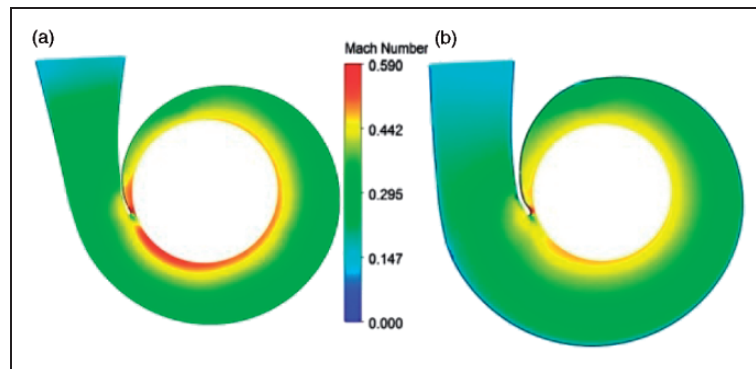


Figure 3. Mach number. (a) Hub-side volute. (b) Shroud-side volute.

tip leakage flows (Figure 2(b)). By varying the rotor grids around the blade surfaces and along the stream-wise and spanwise directions, five mesh sizes were used to predict the turbine performance which stabilized above a grid size of 2.9 million of nodes.

The ANSYS-CFX-Solver was used to solve the 3D Reynolds-stress-averaged Navier–Stokes equations with mass-averaged velocity and time-averaged density, pressure and energy. The flow in the volute was solved in a stationary frame and that of rotor in a rotating frame. The space before the rotor blade leading edge (SLE) is related to the real clearance between the volute exit and the blade leading edge (about 0.4mm) while the space after the trailing edge (STE) is chosen to cover the volume delimited by the rotor axis and the casing. Considering the definition of mean chord length,

$$c_{mean} = \sqrt{(x_{rot} - \frac{h_{in}}{2})^2 + (r_{in} - r_{mean out})^2}$$

the values of SLE and STE are 1.25% and 39.9% of c_{mean} (32.6 mm), respectively. To account for the frame of reference transfer and pitch change between volute exit and rotor inlet, the frozen interface was selected. The boundary conditions considered were a total pressure and a total temperature at a volute inlet and a variable mass flow rate at the draft pipe outlet. The minimum and maximum values of y^+ on the surfaces of the volute and rotor were 0.52–60, but it was difficult to have small values of y^+ near the hub and tongue. In the present flow simulations, the $k-\omega$

Shearing stress turbulence model (SST) with an automatic wall function was considered, with using the wall function when y^+ exceeds 2 and the low Reynolds method for y^+ less than 2.

Steady simulations

First, the frozen rotor simulations were obtained based on a high resolution scheme and a local time step. The following section discusses the flow structures within the volute and the rotor when operating at the design point.

Flow in volute

The streamlines plotted at the mid-span of hub side volute are seen to follow perfectly the volute, but there are non-uniformities observed near the tongue where a part of the infiltrated flow recovers the main flow at rotor entry. Figure 3 depicts the Mach number in the hub and shroud sides of volute, showing that the flow accelerates uniformly till the tongue region. The lower momentum of fluid entering the rotor is due to wake from the tongue and flow mixing between that emerging from under the tongue with that circling the entire rotor. It seems that the influence of the wake and mixing do not extend further than a circumferential angle of 60° from the tongue. Furthermore, the flow velocity is higher near the shroud side than the hub side, at exit of the volute, and subsequently the

swallowing capacity of the shroud rotor region is higher as also described in literature.^{2-4,11-15} Capobianco and Gambarotta³ related this dissimilar behaviour to the difference between the cross-sectional areas of the two entries while Aghaali and Hajilouy-Benisi¹¹ suggested that the blade loading losses are the principal source of mass flow rate differences causing the flow to pass more through the shroud side entry.

The velocity vectors are superimposed on the plot of total pressure at the inter-space (Figure 4) to reveal the flow structures between the shroud side and hub side, seen to affect the flow incidence at the rotor entry and cause high losses, and in practice, the best efficiency is shown to occur at an optimum incidence angle.^{4,5} At a distance of 10% from the divider, there is a decrease in the total pressure through the entire circumference, caused by mixing losses and wakes due to jets from both sides that separate near the lip, as well as a recirculation zone between the tongue and the inlet of inter-space.^{11,12} A comparison between the distance of 10% and 25% shows the same distribution of total pressure with a less wake effect. At a distance of 50%, the effect of recirculation persists, but it is difficult to observe the mixing zone. The tongue effect is depicted by a proportion of infiltrated flow that takes part to feed the rotor, thus creating mixing losses. After a distance of 75%, the wake is dumped by convection, and the tongue effect is clearly

illustrated by a lower stagnation pressure. The vectors of flow velocity depict a mixing zone near the divider and are largely inclined from the radial direction. The flow entering from the shroud-side has an axial component, which by approaching the volute exit tends to vanish except near the tip.

Flow in the rotor

The vectors of relative flow velocity (Figure 5) show a clear vortex caused by a high negative incidence in the rotor entry region. Near the hub pressure corner, there are very low velocities and the flow is re-attaching onto pressure side at mid-span. The running clearance between the blade and the casing seems to let the fluid to traverse from the high pressure side to the low pressure side. Over 70% of blade length, the flow over the tip seems to be more inclined to the streamwise direction and is diverted towards the blade trailing edge.

The spanwise surfaces and cross sections of rotor (Figure 6) exhibit regions of high losses at the inlet and in the tip clearance, which become stronger near the shroud toward the exit of rotor. At the mid of trailing edge, there is a wake due to viscous layers that emerge from both sides of blade. There is a clear region of losses at the rotor outlet due to wake extending from the trailing edge. At 95% spanwise

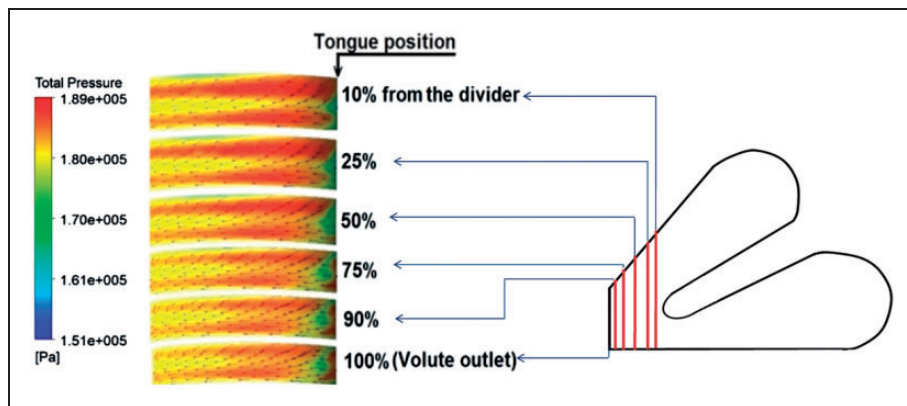


Figure 4. Velocity vectors over total pressure at difference inter-space positions.

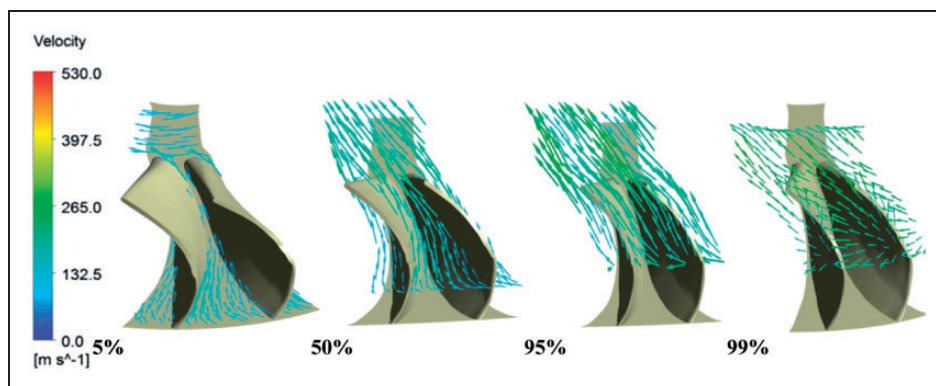


Figure 5. Relative flow velocity vectors at different spans.

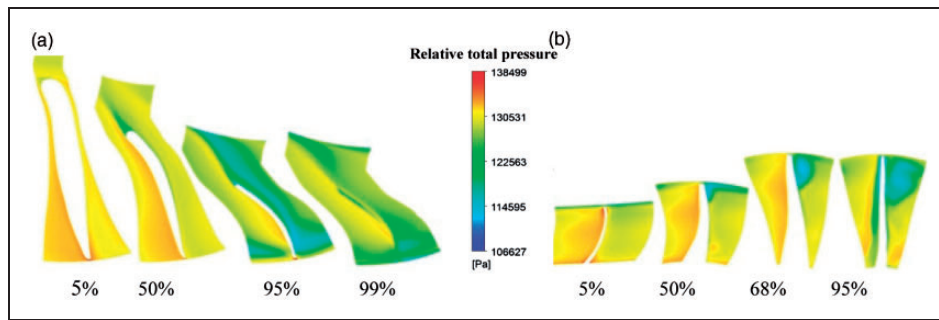


Figure 6. Relative total pressure. (a) Blade span. (b) Cross sections.

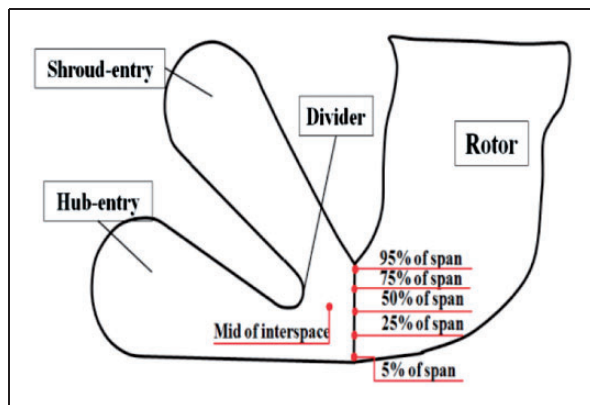


Figure 7. Visualization lines at rotor entry.

(Figure 7), high losses starting from the leading edge are growing up along the blade suction side, mainly caused by the secondary flow and the migration of low energy fluid from the hub to the shroud which interacts with the tip leakage flow. From the leading edge, there is an area of a high loss over the pressure side due to negative incidence which has a strong influence on the rotor flow structure. This not suitable angle produces a vortex that occupies a large part of the channel, thus reducing considerably the efficiency at off-design operation.

The high inclined shroud side entry of this asymmetry twin radial turbine allows the flow entering directly to the inter-space region and then to the rotor, and thus destroying the wake generated by the divider, whereas the volute hub side coincides directly with the inlet hub rotor. A detail description of the flow velocities along the spanwise direction may identify the effect of the volute. Figure 8 shows vectors of relative flow velocity at the rotor entry in several circumferential lines (Figure 8) placed at the rotor inlet for 5%, 25%, 50%, 75% and 95% span. The plans of recording are too close to the blades about 0.4 mm, hence allowing assessing the steady reversed flow along the blade pressure side. The two volute exits present a dissymmetrical behaviour depicted by non-uniformity at the rotor inlet in both spanwise and circumferential directions, in terms of amplitude (Figure 8) and direction (Figure 9) of the relative flow velocity vectors. As seen before, the loss

generated downstream of the divider is more inclined to the hub and the flow velocity is higher in the shroud. In addition, the flow upstream the tongue is turned radially, whereas that at downstream coincides with the mixing region formed by the infiltrated flow and the flow coming from the two entries, which affects the inlet flow condition to the rotor. Also, along the spanwise direction, the inlet rotor is affected by the boundary layer separations from the hub and shroud sides and the wake downstream the divider. According to Figure 10 the average relative flow angles are -38.8° , -37.3° , -35.5° , -25.6° and -21.8° , respectively. Indeed, Baines and Yeo⁵ showed that at an equal admission the incidence angle is close to -30° . There are large variations of steady relative flow angle during the rotor rotations which are from -67° to 39° . Figure 8 reveals that the steady relative flow angle takes a high values around the tongue (before 45° and after 60°), which seems to be highly influenced in the tongue due to the interaction between the main flow and that infiltrated to take part in the feeding of rotor.

Predicting aerodynamic performance

The stage interface simulations based on one-blade computational domain were used to predict the performance map and operating range of this twin-entry radial turbine. The used values of average pressure and temperature at turbine inlet correspond to the real operating conditions at the testing conditions of two Schwitzer turbochargers with a V12 diesel engine by Ghenaiet.²¹ The mass averaging of the thermodynamic properties such as the total enthalpy and other properties is done with respect to the inlet and the outlet planes of the computational domain. The predicted total to static isentropic efficiency and expansion ratio as function of reduced mass flow parameter and rotational speeds, reveal that the design point is close to a mass flow of 0.28 kg/s and a speed of 60,000 r/min (Figure 10(a)), for a maximum efficiency around 72.9%. This design point was also confirmed for the centrifugal compressor of the same turbocharger, according to Khalfallah and Ghenaiet,²² and by comparing them to some available experimental data, the trend in the expansion ratio and the isentropic

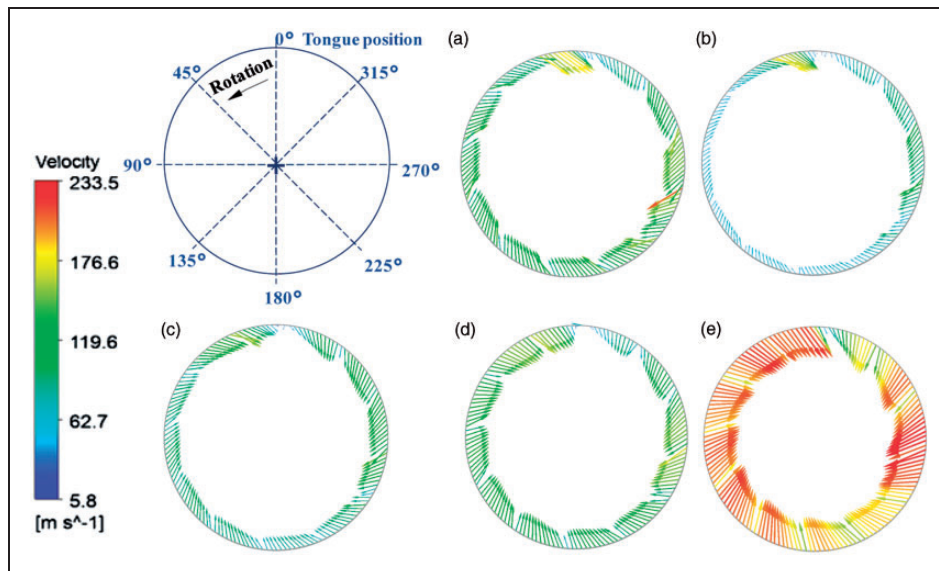


Figure 8. Flow relative velocity vectors at rotor entry at span. (a) 5%, (b) 25%, (c) 50%, (d) 75% and (e) 95% span.

efficiency are similar to those obtained by Aghaali and Hajilouy-Benisi¹¹ and Romagnoli et al.²³ The choked regime is recognized by the vertical portion of characteristics (Figure 10(b)) that corresponds to a reduced mass flow of 6.47×10^{-5} (mass flow = 0.401 kg/s and for 60,000 r/min). The maximum isentropic efficiency at each rotational speed is shown to be close to a velocity ratio of 0.707 (Figure 10(c)) which is near the theoretical value.

Unsteady simulations

The development of the instabilities inside turbomachines is negatively affecting the performance in terms of efficiency, vibrations, stability and noise emission. According to the open literature, the main research on twin radial turbines is directed towards assessing their aerodynamic performance and the developments of prediction models.^{2,3,12,14,17,18} The unsteady flow field measurements in the volute-rotor interface are rare due to the great demands on the measurement techniques, especially concerning the pulsating behaviour of flows accompanied by high a rotational speeds, and there are only few researches found with a good agreement between experimentation and theory at a low rotational speed.^{24,25} The present study constitutes an attempt to introduce the aeroacoustic theory of Tyler and Sofrin²⁶ to characterize the phenomena of interactions between components. This theory considers the pressure fluctuations as “a superposition of effects” which may be thought as viscous and potential effects, and notes the existence of a spinning mode by considering the superposition of any kind of perturbations. Accordingly, the transient rotor/stator interface is used to account for these transient interaction effects. The transient relative motion on each side of the general grid interface (GGI) connection is simulated and the interface

position is updated at each time step, as the relative position on each side of the interface varies with time. The used transient scheme is the second-order backward Euler with an automatic time step initialization. The time step was set at $4.16 \mu\text{s}$ corresponding to angular displacement of 1.5° . The solver performs a number of 20 iterations for each time step which was sufficient to get a residual inferior to 10^{-5} . The total time simulation corresponds to two rounds of rotor, which required substantial computations resources. It should be recalled that the steady state computations were run beforehand to produce the starting results.

Spectral analyses

The pressure fluctuations were recorded along circumferential lines at different spanwise positions passing by the tongue and at the volute/rotor interface plane. The interactions phenomena produced by the movement of the rotor blades against the volute tongue are defined in the chorochronic periodicity model stipulating that the signal corresponding to each aerodynamic property emerging from the interaction can be represented by a superposition of infinity of rotating waves, and hence all the matter is to describe these rotating waves. This model originates from the fact that the flow is characterized by a spatial and time (double) periodicity, as explained by Gerolymos et al.²⁷ For example, the static pressure presents a space and a time periodicities as follows

$$p(t, \theta, x, r) = p(t, \theta + \Delta\theta, x, r) = p(t + \Delta t, \theta, x, r) \quad (1)$$

For a radial turbine with full blades row, the period is equal to 2π , if the greatest common divider (GCD) of N_{rot} and N_{stat} (numbers of rotating and stationary blades) is equal to 1. A particular case happens when

this GCD is different from 1, and in the case where a passage of N_{rot}/GCD blades of the rotating row and a passage of N_{stat}/GCD of stationary blades have the same pitch, hence the spatial period is equal to

$$\Delta\theta = \frac{2\pi}{\text{GCD}} \quad (2)$$

The angular frequencies of the modes in the stator frame depend only on the rotor harmonics n . For example $n=1$ gives the rotor blade passing frequency (BPF) and the higher values yield multiples of it

$$\omega_n = nN_{rot}\Omega_{rot} \quad (3)$$

Indeed, the static pressure can be described by the double Fourier decomposition as proposed by Tyler and Sofrin²⁶

$$p(x, r, t, \theta) = \sum_{n=0}^{+\infty} \sum_{m=-\infty}^{+\infty} P_{mn}(x, r) e^{i[m\theta - nN_{rot}\Omega_{rot}t + \varphi_{mn}]} \quad (4)$$

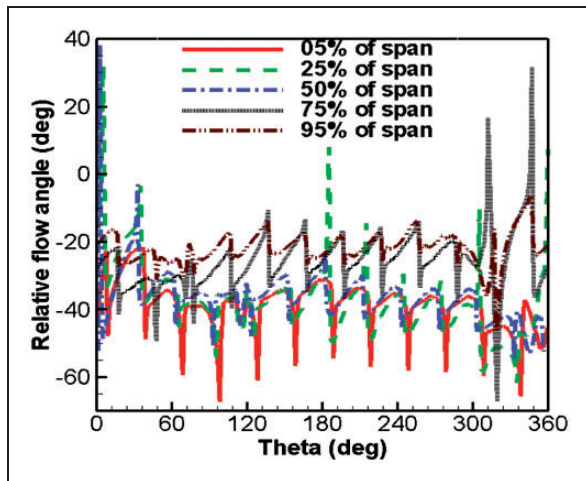


Figure 9. Relative flow angle.

The sum is modelled as a superposition of infinity of rotating waves, characterized by a phase φ_{mn} and an amplitude $P_{mn}(x, r)$, and the rotating velocity is given by

$$\Omega_m = nN_{rot}\Omega_{rot}/m \quad (5)$$

Furthermore, it was shown that the mode m , also called spinning mode, of the spatial Fourier decomposition is given by

$$m = nN_{rot} + kN_{stat} \quad k = \dots, -1, 0, 1, \dots, \quad (6)$$

This equation gives information about what kind of deterministic flow disturbances that can be created from the interaction between a set of two blade rows, with N_{rot} number of rotor blades and N_{stat} number of stator vanes. The disturbances are divided into circumferential modes m (or spinning modes) created from the rotor alone such as $m = nN_{rot}$, and the flow is periodic and stationary in the rotor frame if the turbulent fluctuations are averaged. When these modes, e.g. rotor wakes, interact with the stator vanes, all combinations of modes according to equation (6) occur. The sign of m determines the spinning direction of each mode. Considering the case $n=1$ related to the first harmonic of the blade passing frequency, the pressure fluctuation in equation (4) can be interpreted as a superposition of an infinite number of rotating patterns, where the number of lobes or spinning mode is given by limited values of m (equation 6) and the rotating velocity is given by

$$\Omega_m = N_{rot}\Omega_{rot}/m$$

Considering the present radial turbine where the twin-entry volute acts as a single vane and the number of the rotor is 12, the number of mode m is given by

$$m = 12 + k \quad k = \dots, -1, 0, 1, \dots, \text{ so} \\ m = \dots, 11, 12, 13, \dots,$$

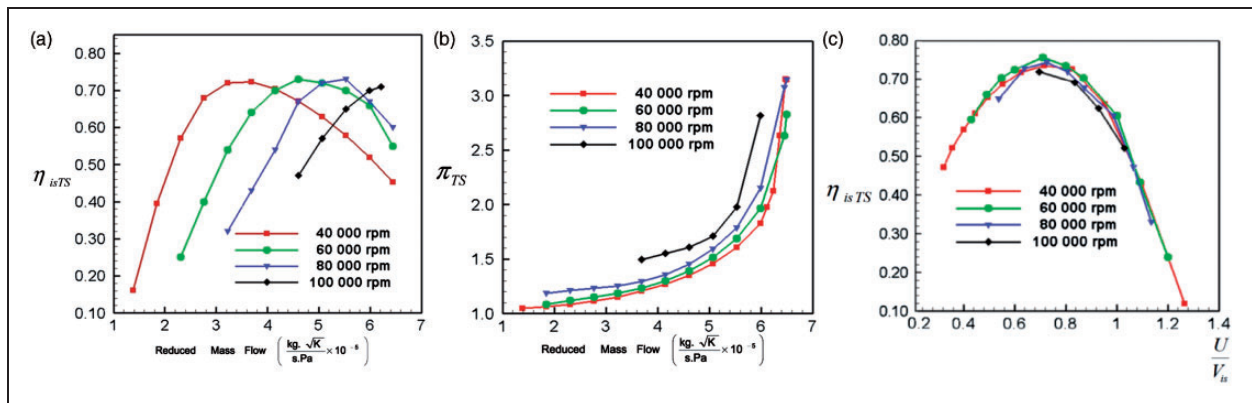


Figure 10. Radial turbine performance. (a) Total-to-static isentropic efficiency, (b) Total-to-static expansion ratio and (c) Isentropic total-to-static efficiency versus (U/V_{is}) .

On the contrary to an axial turbine where the spinning modes are restricted to some particular values (reference), this vaneless twin radial turbine is characterized by the presence of all rotating lobes. The analysis of interactions aimed at identifying the dominating modes and their parameters such as amplitude and rotational speed. Because it is hard to observe these properties in the time domain, an analysis in the frequency domain is performed for the recorded signals of static pressure by applying the FFT.

Non-pulsating flow simulations

In a previous work by Cerdoun and Ghenaiet,²⁸ the unsteady simulations using one blade and full rotor of a twin radial turbine were carried out by emphasizing on the modes of components interactions and noticing the difference between them. The results show clearly that the one-blade passage simulation could not detect important modes, in addition there is decaying amplitudes for many harmonics. The one-blade simulation seems to detect only the modes defined by harmonics greater than the number of rotor blades in the volute/rotor interface such as mode 12, and overestimates the amplitudes of all modes inside the volute and rotor. Also, the effect of tongue represented by the mode $m=1$ is not detected when considering the volute/rotor interface. Inside the volute, both simulations detected the same modes and revealed that the tongue effect is more dominating in the interspaces than in the volute/rotor interface. On the other

hand, the full rotor simulations was able to detect all modes even with harmonics less than the number of rotor blades and their amplitudes seem to be more reasonable compared to one-rotor passage simulation.

In the present study, the transient simulations of the full blades rotor were performed, considering the non-pulsating and pulsating flows for the operating conditions: $N=60,000$ r/min, $m=0.28$ kg/s. The spatial signals of static pressure were recorded along circumferential lines, as seen from Figure 11, located at 25%, 50% and 75% span of the interfaces: volute/rotor and the mid inter-space while the temporal signals were recorded at the tongue and after the tongue in the mid inter-space about 30° from the tongue.

The recorded signals illustrate highly fluctuating static pressure about 90° and 30° forward and backward to the tongue, bringing out the non-uniformity of the flow at the exit of volute, for which most of the zero dimensional (0D) or one-dimensional (1D) models used in predicting the radial turbine performance ignore or neglect. Chen et al.,²⁹ in order to consider this effect, introduced a circumferential variation in losses in their modelling of a twin radial turbine. The present analyses to examine the interactions modes produced by the relative movement of blades against the volute, especially at the tongue, based on the chronochronic periodicity model. This latter stipulates that the signal corresponding to the static pressure emerging from these interactions can be represented by a superposition of infinity of

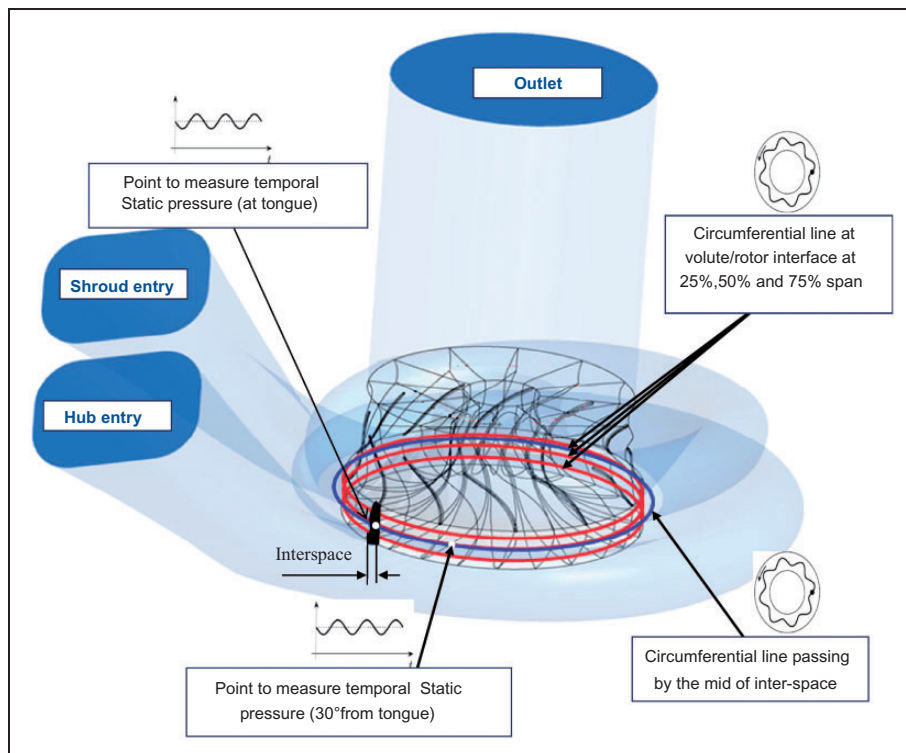


Figure 11. Recording positions of the spatial and temporal static pressure signals.

rotating waves, and hence all the matter is to describe these waves. The use of FFT for the temporal pressure signals allows characterizing the different frequencies of the machine and their evolution in time, whereas that for spatial pressure signals allow determining the essential parameters characterizing these interactions phenomena, which are the amplitude and the rotation speed of different spatial modes (rotating mode) and the most dominant. An example of spatial pressure signal recorded at mid span close to tongue and its subsequent FFT spectrum at an instant equal to 2 ms are presented in Figure 12, revealing the potential effect related to the tongue acting as a single vane. Furthermore, the static pressure signals at circumference lines passing by the mid of divider inter-space and rotor include the effect of both the wake generated in the mixing zone between the two entries, to cause a deficit in total pressure. The rotor blade passing frequency and the spinning mode 2 may be described as the interaction between the rotor and the two entries. Also, the harmonic 12 related to the potential effect of the rotor is dominant in this area, and it is difficult to make a distinction between this harmonic and the multiples of harmonic 1. The rotational speed and the harmonic range of this lobed structure are calculated from equation (5), giving $\Omega_m = \Omega_{rot} = 60,000$ r/min. This mode, which is dumped and not convected through the rotor passage, represents the potential effect of the rotor blade that would be the unique existing mode in an isolated rotor. Even though the recording line is about 4 mm before the leading edge of the blade rotor (simulated in the stationary frame), the flow is shown to be significantly affected by the passing blade. According to the measurements of Karamanis et al.,⁶ in a plane at 3 mm upstream the rotor leading edge this effect was shown to persist.

FFT analysis of pressure signals recorded at the volute/rotor interface along circumference lines at 25%, 50% and 75% span (Figure 13), are all depicting a dominating harmonic 12 that reveals the potential effect of the rotor and another defined by harmonic 1 related to the tongue. The difference lies

in the magnitude of these modes: 0.58 bar, 0.73 bar and 0.95 bar for the circumference lines at 25%, 50% and 75% span, respectively, which are more dominating near the shroud due to the blade tip effect.

The spectrum resulting from FFT analysis of the temporal pressure fluctuations as recorded before, at and after the tongue and at the volute/rotor interface, depict a first peak value of 1000 Hz corresponding to the frequency of the tongue. According to Figure 14, the periodic effect corresponds to the flow events undergone by rotor at BPF equal to 12,000 Hz that corresponds to the blades number multiplied by the rotor frequency. The first harmonic 24,000 Hz is the multiple of BPF.

Pulsatile flow simulations

Ehrlich³⁰ performed extensive measurements on a diesel engine with an in-line six-cylinders medium speed with a quite low output (5.9 l, peak torque 569 Nm at 1600 r/min) to analyze the on engine turbine performance under pulsatile flow. He measured the instantaneous total and static pressure at both inlet and outlet of the twin-entry turbine using in-house constructed probes connected to a high frequency dynamic pressure transducer. The velocity field in the horizontal central plane was measured by particle image velocimetry (PIV), at chosen crank angles during the engine cycle to characterize the turbine inlet velocity profile during an exhaust valve event. The exhaust gases are ducted away from the turbocharger turbine and discharged outside the test cell. The butterfly valves installed in the intake air and exhaust gas ducts set an inlet restriction and an exhaust backpressure, respectively. When this Schwitzer turbocharger was tested with a heavy truck V12 diesel engine,²¹ the inlet and outlet average steady value of pressure and temperature were measured. By combining these two experimental results (average values from,²¹ and instantaneous values from³⁰), the present scaled boundary conditions were imposed. The pulsating flow was imposed at each entry of the volute (Figure 16(a) and (b)), by

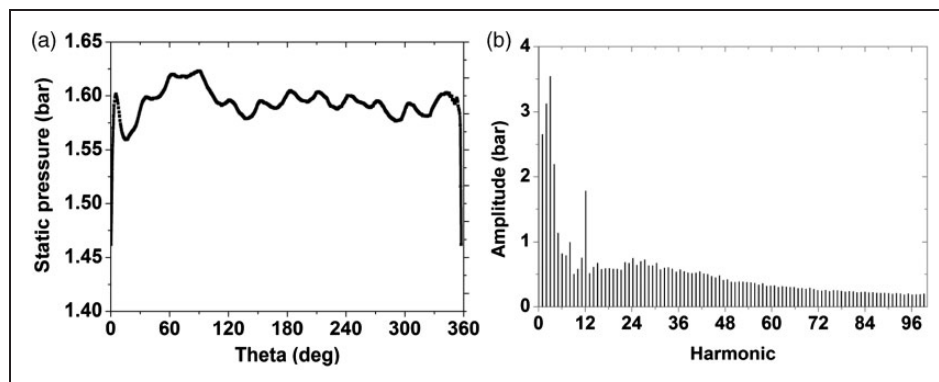


Figure 12. Spectrums of spatial pressure fluctuations near tongue.

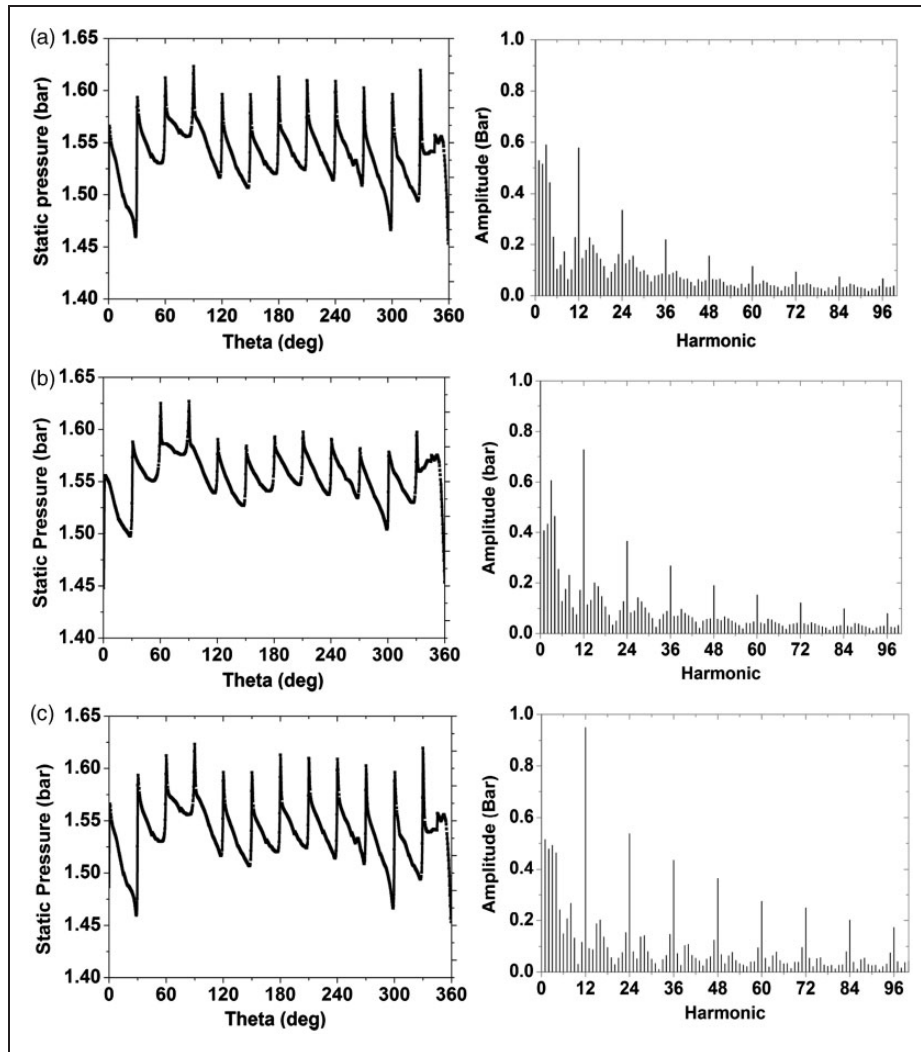


Figure 13. Spectrums of spatial pressure at rotor/volute at. (a) 25% span, (b) 50% span and (c) span 75%.

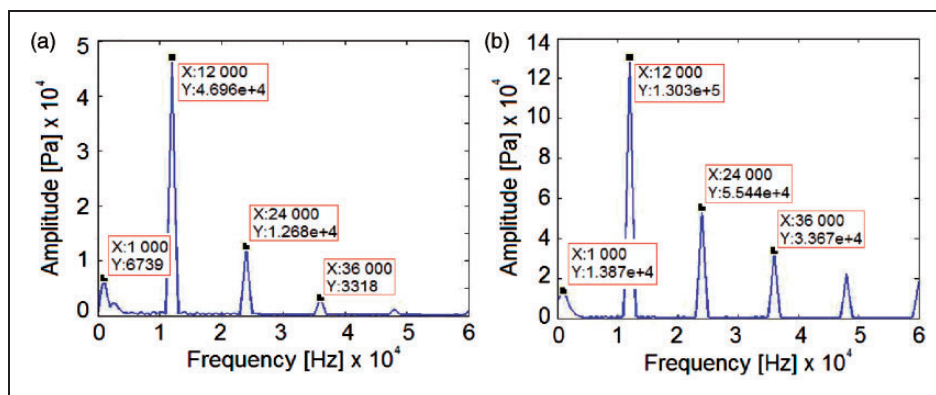


Figure 14. Spectrums of temporal pressure fluctuations. (a) At tongue. (b) At volute/rotor interface.

considering the total temperatures $T_{t_{meas}}$ and total pressures $P_{t_{meas}}$,³⁰ (see Figure 15(a) and 15(b)) scaled by the measured average of total pressure and total temperature ($P_{t_{ave}}, T_{t_{ave}}$)²¹ and the actual rotational speed of the heavy truck diesel engine, and by verifying equations (7) and (8)

$$P_t = P_{t_{meas}} + \left(P_{t_{ave}} - \frac{1}{2\pi} \int_0^{2\pi} P_{t_{meas}} \cdot d\theta \right) \quad (7)$$

$$T_t = T_{t_{meas}} + \left(T_{t_{ave}} - \frac{1}{2\pi} \int_0^{2\pi} T_{t_{meas}} \cdot d\theta \right) \quad (8)$$

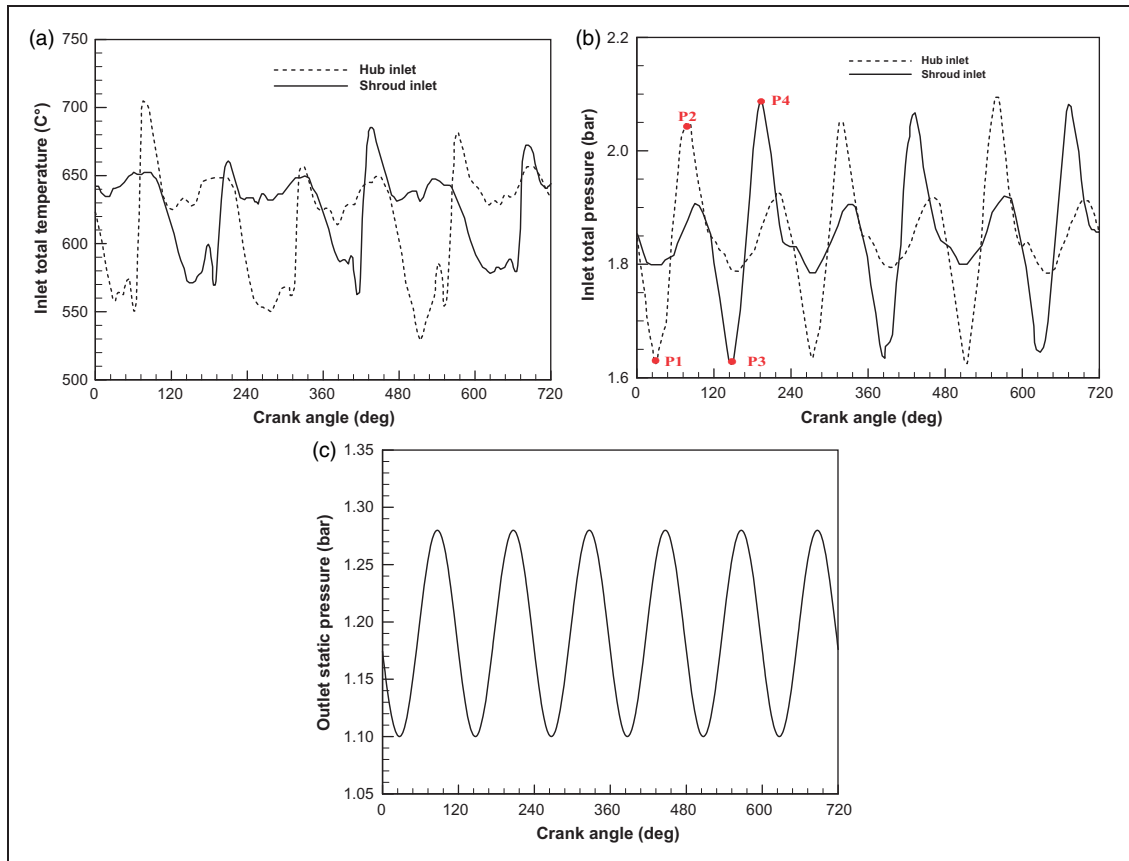


Figure 15. Boundary conditions. (a) Inlet total pressure, (b) Inlet total temperature and (c) Outlet static pressure.

At the exit from turbine, Ehrlich³⁰ showed that the static pressure perturbation (shown by Figure 15(c)) is nearly sinusoidal for both low and high loads and it is characterized by six pulses per engine cycle, corresponding to one valve event in the six-cylinder engine. As aforementioned for the total temperature and total pressure, the static pressure is chosen to verify the following equation

$$P = P_{meas} + \left(P_{ave} - \frac{1}{2\pi} \int_0^{2\pi} P_{meas} \cdot d\theta \right) \quad (9)$$

The present adapted boundary conditions are deemed sufficient to carry out the pulsating flow simulations.

The used time-step for the present unsteady simulations is $4.67 \mu\text{s}$ corresponding to a wheel rotation of approximately 1.5° . Figure 16 presents the static pressure signals recorded at the mid inter-space from the divider and their FFT analyses applied to the unsteady field at distinctive instants. Indeed P1 is an equivalent instant that corresponds to the minimum of pressure at hub-side entry and P2 to the maximum while P3 corresponds to the minimum of pressure at shroud-side entry and P4 to its maximum. The flow behaviour resulting from the pulsatile flow condition is naturally highly fluctuating, and according to four instants (P1, P2, P3 and P4), the velocity, the static pressure and the mass flow are highly non-uniform

through the two entries, thereby a leakage flow from the throat side at low pressure to the high pressure side occurs and provokes a flow separation which is convected across the rotor blades, as explained by Katsuyuki et al.³¹ The downstream of the tongue is an area of complex interaction between the wake generated by the flow dissymmetry between the two sides and the proportion of the flow infiltrating to feed the rotor, hence creating a mixing loss between the main flow and the infiltrated flow. By using the spatial Fourier decomposition, the spinning lobe that reveals the tongue effect is identified. Indeed, FFT spectrums show that the interactions are composed by the harmonic 1 and its multiples related to the tongue. Signals recorded at different spans' circumferential lines, reveal a dominant mode $m=2$ (considering $k=-10$) of an amplitude about 1 bar and the mode $m=3$ (considering $k=-9$), resulting from the interaction between the rotor and the tongue which are characterized by spinning modes of rotational velocity $\Omega_2 = 6\Omega$ and $\Omega_3 = 4\Omega$. Furthermore, as noticed the potential effect related to the tongue as represented by the mode 1 dominates the potential effect of the rotor as represented by the harmonic 12.

Figure 17 showing the spatial static pressure recorded along circumferential lines at 25%, 50% and 75% span at the volute/rotor interface just upstream the rotor, depict a periodic behaviour and

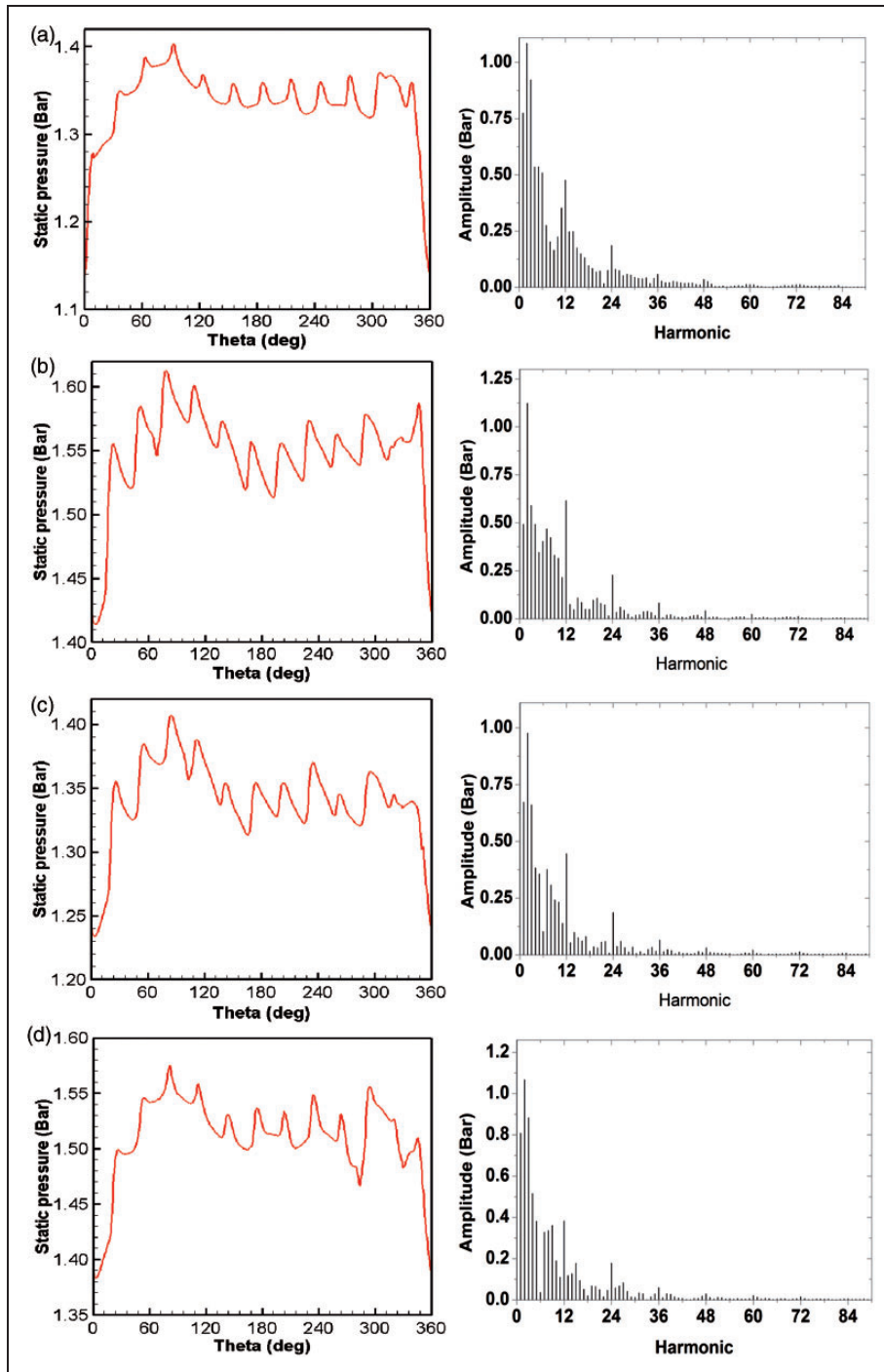


Figure 16. Spatial static pressure fluctuations and corresponding FFT spectrums, at circumference line passing by the mid of divider inter-space at instants. (a) P1, (b) P2, (c) P3 and (d) P4.

the effect of tongue is well illustrated. The spectrums related to the signal of static pressure recorded at the volute/rotor interface at the instants P1, P2, P3 and P4 (defined formerly) depict emergence of the rotor effect as represented by the mode 12 and its multiples, which seem to have the same behaviour as with non-pulsating since they are obtained at a fixed instant. Nevertheless, the spinning mode $m=2$ (considering $k=-10$) as related to the interaction between the rotor and the tongue is more dominating than the rotor potential effect as represented by the spinning

mode $m=12$. The behaviour of pressure signals is seen to be highly fluctuating forward the tongue about 60° and backward about 30° . All FFT spectrums reveal that the harmonic 2 is the highest mode that represents the rotor/volute interaction, which is a combination between the rotor blade and the tongue. The harmonic 12 is seen to be dominated by the tongue potential effect and it is difficult to make any distinction between this harmonic and the multiples of harmonic 1, and it is clear that the amplitude of this mode is more dominant as compared to

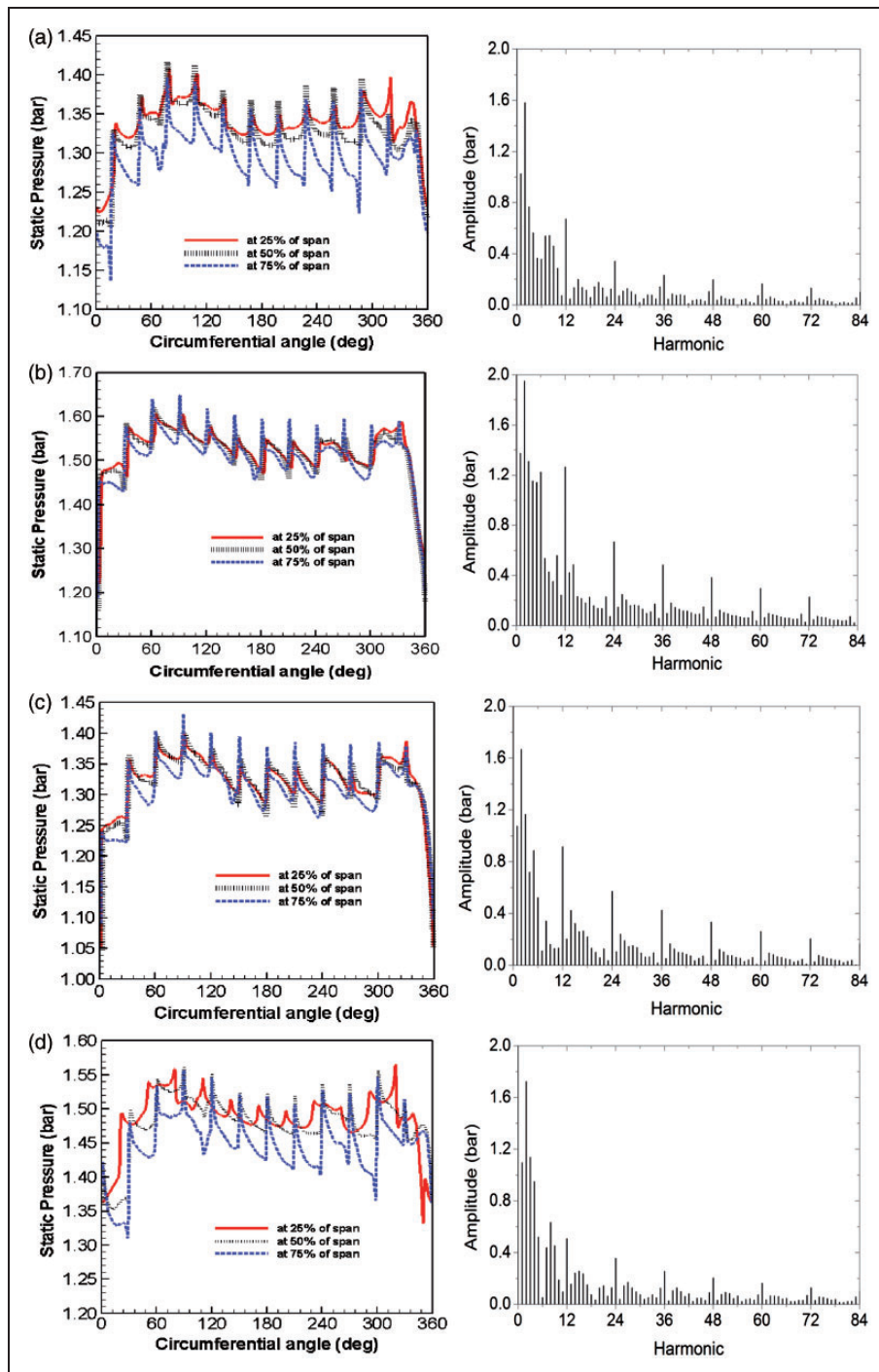


Figure 17. Circumferential pressure signals at rotor/volute interface upstream rotor at 25%, 50% and 75% of span and FFT spectrums are given for 50% span at instants (a) P1, (b) P2, (c) P3 and (d) P4.

other modes, especially near the shroud due to superimposed tip effect.

The temporal static pressure fluctuations obtained with present transient simulations and recorded at the tongue and mid of inter-space about 30° from the tongue (Figure 18) depict a periodic character corresponding to the flow events undergone by the blades at BPF (higher harmonics) equal to 12,000 Hz related to the rotor blades number (12) multiplied by the rotor frequency (1000 Hz). Analysis of temporal signals recorded at the interspace, allowed to detect

three higher values of frequency related to the frequency of the pulsatile flow and their two first multiples in addition to the lower frequencies representing the BPF and their multiples. Such a dominance of the pulses frequency has been confirmed in previous researches,^{32–34} suggesting that the volute is the main source of the non-quasi-steadiness of the flow given its length and volume as compared to other components of turbine.

The obtained results from the spatial analyses in both non-pulsatile and pulsatile flow simulations

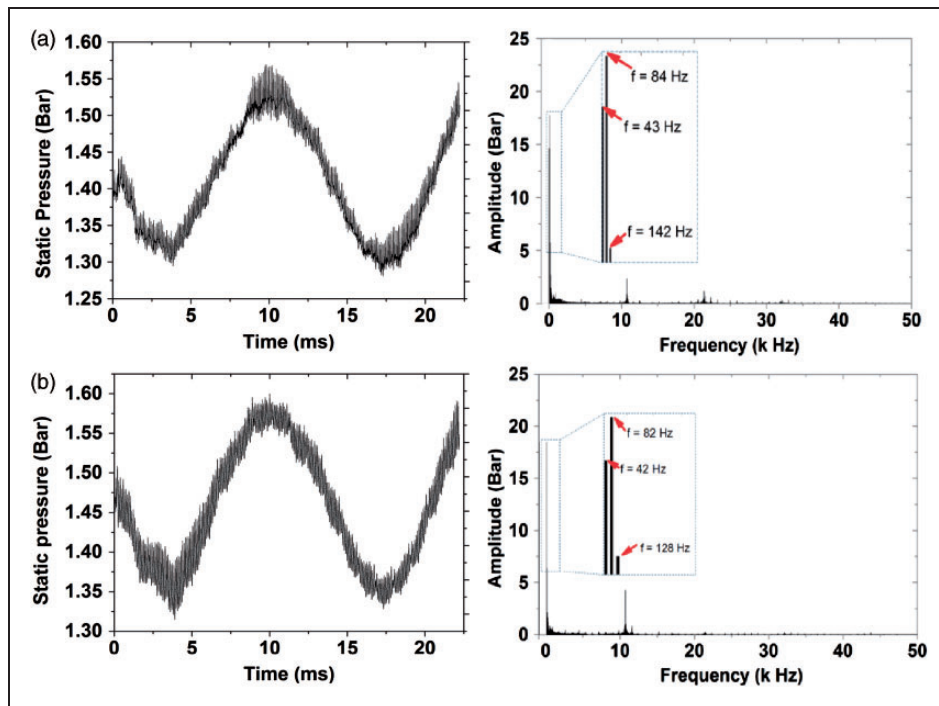


Figure 18. Spectrum of temporal FFT of Static pressure fluctuations at different point. (a) Tongue. (b) Mid of inter-space 30° from tongue.

reveal the dominance of the tongue effect. Relatively to the inter-space the tongue effect is more apparent in case of pulsatile flows, but the difference resides in the amplitude of the lobed structure. The mode 12 and its multiples are dumped quickly in the case of pulsatile flow simulations. FFT spectrums of temporal static pressure depict a pulsating frequency of an amplitude higher than that of BPF; especially at forward inter-space, thus revealing the pulsating character of the flow in the volute. Finally, the comparison between the pulsatile and non-pulsatile flow shows differences with respect to the temporal analysis, whereas in the spatial analysis, the same modes are observed and the difference resides only in the amplitudes of these modes.

Conclusion

The steady and transient flow simulations through the components of this twin-entry radial turbine have produced a good insight into the complex flow structures. Firstly, the influence of the tongue is depicted by a low momentum of fluid entering the rotor and a flow mixing extending till an angle of 60° . Secondly, the inter-space region is characterized by losses due to mixing between the shroud-side flow and hub-side flow at the divider. The spectral analyses of pressure fluctuations have revealed a space-time periodicity for the case of transient simulations with either non-pulsatile flow or pulsatile flow at the inlet. Also, the space modes and rotational speeds and amplitudes characterizing this unsteadiness are determined. The volute/rotor interactions are clearly revealed through existing

rotor and tongue potential effects represented by the spinning modes 12 and 1. In the case of pulsating flows the temporal analysis revealed the dominance of the pulse frequency and multiples against the BPF, and the interaction between tongue and rotor seems to be more dominant. For different unequal admissions, the spectral analyses of pressure fluctuations recorded at the inter-space seem to have the same behaviour since the spatial signals are obtained at a fixed instant.

Conflict of interest

None declared.

Funding

This research received no specific grant from any funding agency in the public, commercial, or not-for-profit sectors.

References

1. Pischinger F and Wunsche A. The characteristic behaviour of radial turbines and its influence on the turbocharging process. In: *CIMAC Conference*, Tokyo, 1977, pp.545–568.
2. Dale A and Watson N. Vaneless radial turbocharger turbine performance. *IMEchE*, 1986; C110/86: 65–76.
3. Capobianco M and Gambarotta A. Performance of a twin-entry automotive turbocharger turbine. *ASME paper* 93-ICE-2, 1993.
4. Yeo JH and Baines NC. Pulsating flow behaviour in a twin-entry vaneless radial-inflow turbine. *IMEchE paper* no. C405/004/90, 1990.
5. Baines NC and Yeo JH. Flow in a radial turbine under equal and partial admission conditions. *IMEchE paper* no. C423/002/91, 1991.

6. Karamanis N, Martinez-Botas RF and Su CC. Mixed flow turbines: inlet and exit flow under steady and pulsating conditions. *J Turbomach ASME* 2001; 123: 359.
7. Hakeem I, Su CC, Costall A, et al. Effect of volute geometry on the steady and unsteady performance of mixed-flow turbines. *Proc IMechE, Part A: J Power and Energy* 2007; 221: 535–549.
8. Simpson AT, Spence SWT and Watterson JK. A comparison of the flow structures and losses within vaned and vaneless stators for radial turbines. *ASME J Turbomach* 2009; 131: 031010–1.
9. Simpson A, Spence SWT, and Early J. A numerical and experimental study of the rotor inlet flow fields of radial turbines using vaned and vaneless stators. ASME paper no. GT2009-59998, 2009.
10. Spence S, Rosborough R, Artt D, et al. A direct performance comparison of vaned and vaneless stators of radial turbines. *J Turbomach* 2007; 129: 53–61.
11. Aghaali H and Hajilouy-Benisi A. Experimental modelling of twin-entry radial turbine. *IJST Iran J Sci Technol Trans B Eng* 2008; 32: 571–584.
12. Hajilouy-Benisi A, Rad M and Shahhosseini MR. Modelling of twin-entry radial turbine performance characteristics based on experimental investigation under full and partial admission conditions. *Mech Eng* 2009; 16: 281–290.
13. Hellström F and Fuchs L. Numerical computations of pulsatile flow in a turbo-charger. 46th AIAA paper AIAA-2008-073, 2008.
14. Hellström F and Fuchs L. Effects of inlet conditions on the turbine performance of a radial turbine. ASME paper GT2008-51088, 2008.
15. Hellström F and Fuchs L. Numerical computation of the pulsatile flow in a turbocharger with realistic inflow conditions from an exhaust manifold. ASME paper GT2009-59619, 2009.
16. Costall AW, McDavid RM, Martinez-Botas RF, et al. Pulse performance modelling of a twin entry turbocharger turbine under full and unequal admission. *J Turbomach ASME* 2011; 133: 021005–1.
17. Copeland CD, Martinez-Botas RF and Martin S. Unsteady performance of a double entry turbocharger turbine with a comparison to steady flow conditions. *J Turbomach ASME* 2012; 134: 021022–1.
18. Romagnoli A, Copeland CD, Martinez-Botas RF, et al. Comparison between the steady performance of double-entry and twin-entry turbocharger turbines. *J Turbomach ASME* 2012; 135: 011042–11.
19. Moser M, Tapken U, Enghardt L, et al. An investigation of low pressure turbine blade-vane interaction noise: measurements in a 1.5-stage rig. *Proc IMechE, Part A* 2009; 223: 687–695.
20. Enghardt L, Tapken U, Neise W, et al. Turbine blade/vane interaction noise: acoustic mode analysis using inlet duct sensor rakes. In: *Proceedings of the seventh AIAA/CEAS-aeroacoustics conference*, Maastricht, The Netherlands, 28–30 May, paper no. 2001–2153.
21. Ghenaïet A. Predicting the aerodynamic performance of turbocharger components. In: *IMechE, compressors and their systems*, 2007, paper no. C658/010/07. Oxford, UK: Chandos Publishing.
22. Khalfallah S and Ghenaïet A. Impeller-vaneless-diffuser-scroll interactions and unsteady flow analysis in a centrifugal compressor. *IMechE, compressors and their systems*, 2009, paper no. L20/C682/020. Oxford, UK: Chandos Publishing.
23. Romagnoli A, Martinez-Botas RF and Rajoo S. Steady state performance evaluation of variable geometry twin-entry turbine. *Int J Heat Fluid Flow* 2011; 32: 477–489.
24. Binder A, Förster W, Kruse H, et al. Experimental investigation into the effect of wakes on the unsteady turbine rotor flow. *ASME J Eng Gas Turbine Power* 1985; 107: 458–465.
25. Lengani D, Paradiso B, Marn A, et al. Identification of spinning mode in the unsteady flow field of a low pressure turbine. *J Turbomach ASME* 2012; 134: 051032–1.
26. Tyler JM and Sofrin TG. Axial flow compressor noise studies. *SAE Trans* 1962; 70: 309–332.
27. Gerolymos GA, Michon GJ and Neubauer J. Analysis and application of chorochronic periodicity in turbomachinery rotor/stator interaction computations. *J Propul Power* 2002; 18: 1139–1152.
28. Cerdoun M and Ghenaïet A. CFD analyses of a radial inflow turbine. In: *IMechE, 8th international conference on compressors and their systems*, 2013, pp. 635–647.
29. Chen H, Hakeem I and Martinez-Botas RF. Modelling of a turbocharger turbine under pulsating inlet conditions. *Proc IMechE, Part A: J Power and Energy* 1996; 210: 397–408.
30. Ehrlich DA. *Characterisation of unsteady on-engine turbocharger turbine performance*. Doctoral Thesis, Purdue University, PhD Dissertation, December 1998.
31. Katsuyuki O, Takao Y, Toyotaka Y, et al. Development of twin-scroll turbine for automotive turbochargers using unsteady numerical simulation. *Mitsubishi Heavy Ind Tech Rev* 2013; 50: 23–31.
32. Chen H and Winterbone D. A method to predict performance of vaneless radial turbines under steady and unsteady flow conditions. In: *Proceedings of IMechE*, 1990, paper no. C405/008, pp 13–22.
33. Abidat M, Hachemi M, Hamidou M, et al. Prediction of the steady and non-steady flow performance of a highly loaded mixed flow turbine. *Proc IMechE, Part A: J Power and Energy* 1998; 212: 173–184.
34. Costall A, Szymko S, Martinez-Botas RF, et al. Assessment of unsteady behaviour in turbocharger turbines. In: *Proceedings of ASME turbo expo*, 2006, paper no. GT2006-90348.

Appendix

Notation

BPF	blade passing frequency	
C_{mean}	mean chord	[m]
h_{in}	height of blade at inlet	[m]
M	interaction spatial mode	
N	interaction temporal mode	
N_{rot}	number of rotor blades	
N_{stat}	number of stator blades	
P	pressure	[Pa]
P_{ave}	average outlet pressure	[Pa]
P_{t0}	inlet total pressure	[Pa]
P_{t0_ave}	average total pressure	[Pa]
R	radial coordinate	[m]
r_{in}	radius a rotor inlet	[m]
r_{out}	radius a rotor exit	[m]
T	time	[s]
T_{t0}	inlet total temperature	[K]
T_{t0_ave}	average inlet total temperature	[K]
U	peripheral speed	$[m\ s^{-1}]$
V_{is}	isentropic velocity	$[m\ s^{-1}]$
X	axial coordinate	[m]
X_{rot}	axial rotor length	[m]
$\Delta\theta$	spatial period	[rad]
θ	circumferential coordinate	[rad]
Ω_m	speed of rotation of m th space mode	Ω_m
Ω_{rot}	speed of rotation of rotor	Ω_{rot}